Supporting Information

High Spin Fe^{3+}-Related Bonding Strength and Electron Transfer for Sensitive and Stable SERS Detection

*Xinlu Zheng, Xiao Wu, Letian Zhang, Jianjian Kang, Man Zhou, Yang Zhong, Jinlong Zhang and Lingzhi Wang**

Materials

All the chemicals without note below are analytical grade and used directly without further purification. N, N-Dimethylformamide (DMF, 99.8 wt %), 1,4-benzenedicarboxylate (H_2BDC, 99 wt %), Ethanol (AR), ferric chloride hexahydrate ($FeCl_3 \cdot 6H_2O$), Ferric Chloride Hexahydrate ($NiCl_2 \cdot 6H_2O$) and Titanium isopropoxide (TTIP) were purchased from Sigma-Aldrich.

Characterizations

X-ray powder diffraction (XRD) is analyzed on Rigaku D/max 2250 VB/PC apparatus. Scanning electron microscopy (SEM) images are obtained on TESCAN nova 3. Transmission electron microscopy (TEM) images are recorded on JEOL JEM-2100. XPS measurements were performed on a PHI Quantera XPS scanning microprobe spectrometer with Al Kα (hν = 1486.6 eV) as the x-ray radiation source, which was carefully calibrated on the valence band. Fourier transform infrared spectroscopy (FTIR) was performed on a Nicolet NEXUS 7600 spectrometer. XANES and EXAFS spectra were recorded in the quick scan mode at the BL14B2 facility of SPring-8 at the Japan Synchrotron Radiation Research Institute (JASRI; 8 GeV, 100 mA). The data reduction and analysis of the XAFS spectra were conducted using the Demeter software package (ATHENA and ARTEMIS, respectively). SERS spectra were collected on Raman (Reinshaw invia) using various dye as target molecules at an excitation wavelength of 532 nm.

Experimental Section

Synthesis of MIL-101(Fe): MIL-101(Fe) was fabricated via a simple hydrothermal method reported previously.[1] Typically, 1.351 g $FeCl_3 \cdot 6H_2O$ (5 mmol) was dissolved in 40 mL DMF to obtain solution A; 0.776 g H_2BDC was dissolved in 40 mL DMF to obtain solution B. Then, solution A was added into solution B. After stirring vigorously for 20 min, the mixture was transformed into a hydrothermal Teflon-lined stainless autoclave with a volume of 100 mL and heated at 120℃ for 18 h. Orange solid product was obtained after centrifuging and washing by DMF, ethanol and water for three times, respectively. Finally, the solid was dried at 70℃ for 12 h to obtain MIL-101(Fe).

Synthesis of MIL-101(FeNi): MIL-101(FeNi) with different molar ration of Fe and Ni (Fe:Ni) was prepared as similar as the mentioned above. Taking MIL-101(FeNi) with Fe:Ni molar ratio of 1:1 as an example, 0.676 g $FeCl_3 \cdot 6H_2O$ (2.5 mmol) and 0.595 g $NiCl_2 \cdot 6H_2O$ (2.5 mmol) were dissolved in 40 mL DMF to obtain solution A; 0.776 g H_2BDC was dissolved in 40 mL DMF to obtain solution B. Then, solution A was added into solution B. After stirring vigorously for 20 min, the mixture was transformed into a hydrothermal Teflon-lined stainless autoclave with a volume of 100 mL and heated at 120℃ for 20 h. Light orange solid product was obtained after centrifuging and washing by DMF, ethanol and water for three times, respectively. Finally, the solid was dried at 70℃ for 12 h to obtain MIL-101(FeNi) with Fe:Ni molar ratio of 1:1. Other MIL-101(FeNi) materials with different Fe:Ni molar ratios were prepared by the same procedure except for the different Fe:Ni molar ratios.

Synthesis of MIL-101(FeTi): MIL-101(FeTi) with different ration of Fe and Ti (Fe:Ti) was prepared as similar as the mentioned above. Taking MIL-101(FeTi) with added Ti amount of 1% as an example, 1.351 g $FeCl_3 \cdot 6H_2O$ (5 mmol) and 25 μL TTIP were dissolved in 40 mL DMF to obtain solution A; 0.776 g H_2BDC was dissolved in 40 mL DMF to obtain solution B. Then, solution A was added into solution B. After stirring vigorously for 20 min, the mixture was transformed into a hydrothermal Teflon-lined stainless autoclave with a volume of 100 mL and heated at 120℃ for 20 h. Solid product was obtained after centrifuging and washing by DMF, ethanol and water for three times, respectively. Finally, the solid was dried at 70℃ for 12 h to obtain 1% Ti-doped MIL-

101(FeTi). Other MIL-101(FeTi) materials with different added Ti amounts were prepared by the same procedure except for the different Ti doping amounts.

Synthesis of MIL-101(FeNiTi): MIL-101(FeNiTi) with different ration of Ti was prepared as similar as the mentioned above. Taking MIL-101(FeNiTi) with added Ti amount of 1% as an example, 0.676 g $FeCl_3 \cdot 6H_2O$ (2.5 mmol), 0.595 g $NiCl_2 \cdot 6H_2O$ (2.5 mmol) and 25 μL TTIP were dissolved in 40 mL DMF to obtain solution A; 0.776 g H_2BDC was dissolved in 40 mL DMF to obtain solution B. Then, solution A was added into solution B. After stirring vigorously for 20 min, the mixture was transformed into a hydrothermal Teflon-lined stainless autoclave with a volume of 100 mL and heated at 120℃ for 20 h. Solid product was obtained after centrifuging and washing by DMF, ethanol and water for three times, respectively. Finally, the solid was dried at 70℃ for 12 h to obtain 1% Ti-doped MIL-101(FeNiTi). Other MIL-101(FeNiTi) materials with different added Ti amounts were prepared by the same procedure except for the different Ti doping amounts.

DFT calculations

All the density functional theory (DFT) calculations were performed using Vienna Ab Initio Package (VASP) [2, 3]. Perdew-Burke-Ernzerhof (PBE) form of the generalized gradient approximation (GGA) was employed to describe the exchange-correlation functional [4]. The projected augmented wave (PAW) potentials [5, 6] were chosen to describe the ionic cores and valence electrons were taken into account using a plane wave basis set with a kinetic energy cutoff of 450 eV. Partial occupancies of the Kohn-Sham orbitals were allowed using the Gaussian smearing method and a width of 0.05 eV. The electronic energy was considered self-consistent when the energy change was smaller than 10^{-4} eV. A geometry optimization was considered convergent when the force change was smaller than 0.05 eV/Å. Grimme's DFT-D3 methodology [7] was used to describe the dispersion interactions. The Brillouin zone integral used the surfaces structures of 1×1×1 monkhorst pack K-point sampling.

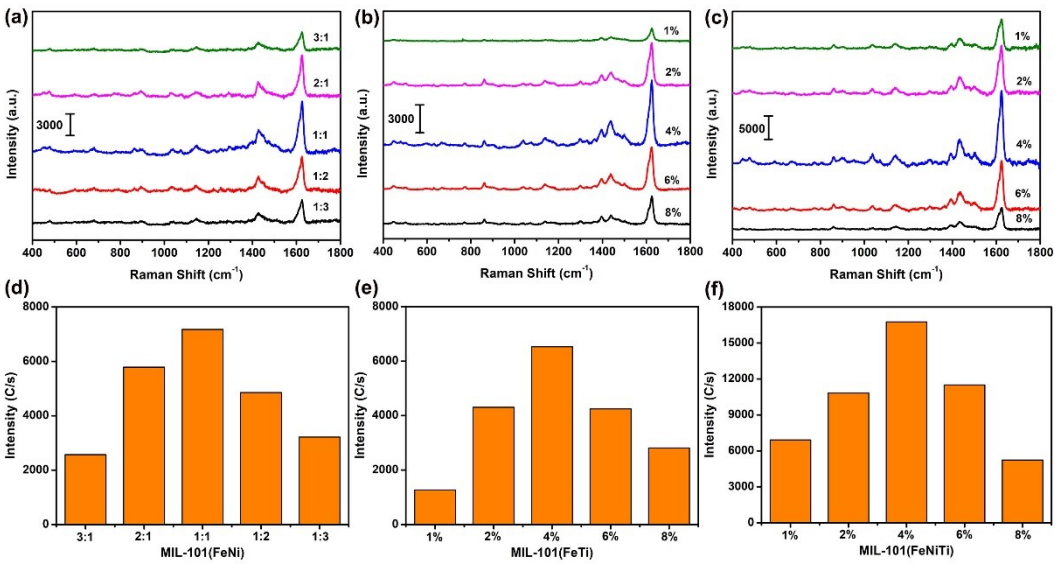

Figure S1. The SERS spectra and the corresponding histogram of MB (10^{-5} M) adsorbed on (a, d) bimetallic MIL-101(FeNi) with different moral ratios of Fe:Ni; (b, e) bimetallic MIL-101(FeTi) with different mass ratios of Ti ions and (c, f) trimetallic MIL-101(FeNiTi) with different ratios mass ratios of Ti ions in MIL-101(FeNi) (1:1 moral ratio of Fe:Ni). Using methylene blue (MB, 10^{-5} M) as the model analyte, the bimetallic MIL-101(FeNi) exhibits a "volcano type" with the increase of Ni amount under 532 nm laser irradiation, where the sample with 1:1 molar ratio presents the most distinguished Raman signal (Figure S1a and 1d). The similar tendency was observed from bimetallic MIL-101(FeTi). The doped Ti amount in MIL-101(FeTi) with the best SERS activity is 4 wt% (Figure S1b and 1e). Based on the above results, different amounts of Ti ions were further added into the MIL-(FeNi) sample with the most outstanding SERS effect (1:1 moral ratio) to figure out the SERS performance of trimetallic MIL-(FeNiTi). As shown in Figure S1c and 1f, trimetallic MIL-(FeNiTi) with the 4 wt% doped Ti presents the strongest SERS intensities. It is noticed the SERS sensitivity can be significantly improved over trimetallic MIL-(FeNiTi).

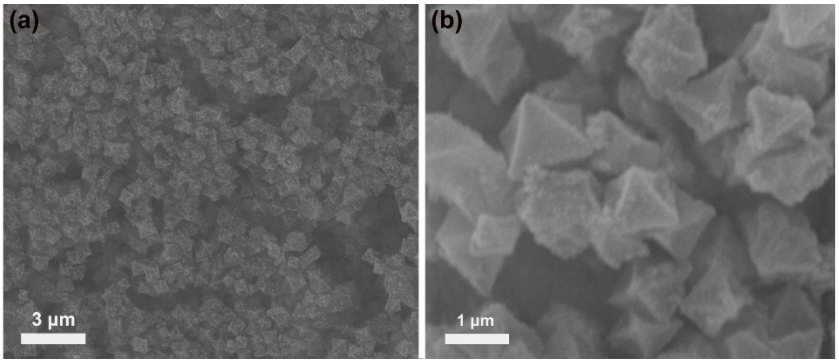

Figure S2. The SEM images of (a) MIL-101(Fe) and (b) bimetallic MIL-101(FeNi).

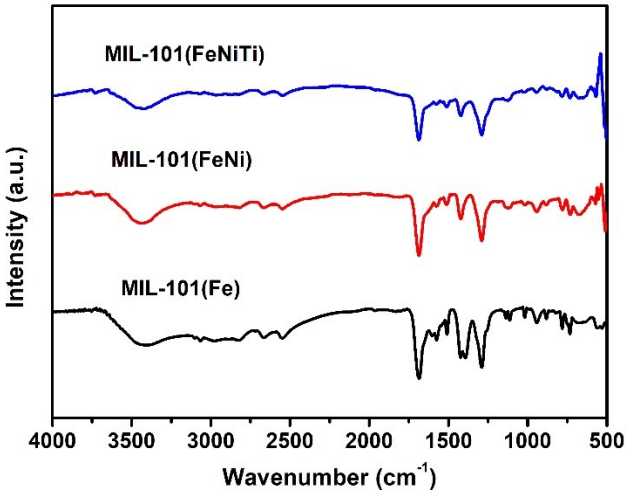

Figure S3. The FT-IR spectra of MIL-101(Fe), bimetallic MIL-101(FeNi) and bimetallic MIL-101(FeNiTi). The characteristic absorption bands at ca. 512 cm^{-1} and 560 cm^{-1} are attributed to the vibration mode of Ni-O and Fe-O, respectively [8, 9]. In the trimetallic MIL-101(FeNiTi) sample, the less obvious signal of Ti-O-C is also detected at ca. 800-950 cm^{-1} due to the presence of little amount of Ti element [10]. Besides, the band at 748 cm^{-1} corresponds to the C-H vibration of the benzene rings. The peaks located at 1389 cm^{-1} and 1601 cm^{-1} belong to the characteristic vibrational bands of the carboxylic acid functional group (O-C-O) in H_2BDC, confirming the introduction of the carboxylic ligand into the prepared MOFs [11, 12]. Furthermore, the absorption peak at ca. 3401 cm^{-1} corresponds to the stretching vibration mode of the O-H. The FT-IR spectra also suggest three kinds of MOFs were accurately synthesized.

The detail of transmission ^{57}Fe Mössbauer spectrum:

It should be noted that not all four-level split bilinear intensities are equal. In general, the strength of hyperfine transitions consists of two contributions, namely:

(1) Items that are independent of angle, that is determined by the square of the Clebsch-Gordan coefficient (referred to as the C coefficient).
If the two nuclear spin states are I_1 and I_2, the corresponding I_x is m_1 and m_2, and their coupling obeys $J= I_1 + I_2$ and $m= m_1 - m_2$. Then the Clebsch-Gordan coefficient is

$$\langle I_1 J - m_1 m \,|\, I_2 m_2 \rangle$$

(2) The angle-related term θ(j, m), which determines the relationship of the relative strength of the transition to the γ-ray propagation direction and the magnetic field direction or the angle θ between the EFG tensor major axes.

The product of the above two items satisfies the following normalization relation:

$\Sigma C^2\theta$(j, m)=1

As for the polycrystalline or powder samples, since the crystallographic axis

orientations are randomly distributed, the relative intensity ratio should be averaged over all values, so:

$$\frac{I\left(\pm\frac{3}{2}\leftrightarrow\pm\frac{1}{2}\right)}{I\left(\pm\frac{1}{2}\leftrightarrow\pm\frac{1}{2}\right)}=\frac{\int_0^x(1+cos^2x)sin\theta d\theta}{\int_0^x(\frac{5}{3}-cos^2x)sin\theta d\theta}=1$$

The absorption spectral area A of a Mössbauer spectrum is proportional to f_a, which is given in the Debye theory by the following formula: [13]

$$f_a(T)=\exp\{-\frac{3}{4}\frac{E_\gamma^2}{Mc^2k_B\theta D}[1+4(\frac{T}{\theta D})\int_0^{\theta D/T}\frac{xdx}{e^x-1}]\}$$

where M is the mass of the Mössbauer nucleus, c is the speed of light, Eγ is the energy of the Mössbauer transition, and θD is the Debye temperature.

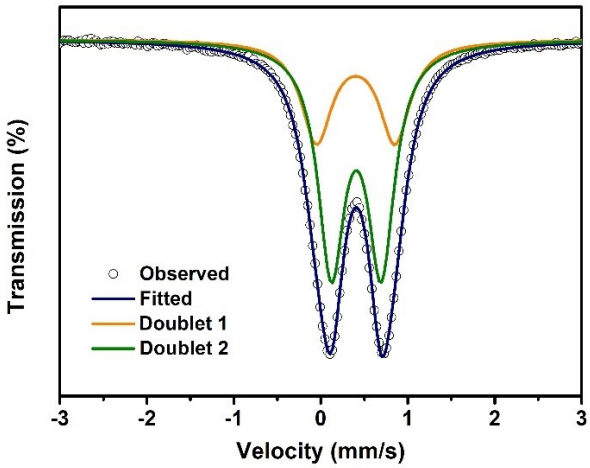

Figure S4. [57]Fe-Mossbauer spectroscopy of bimetallic MIL-101(FeTi) with the best SERS activity.

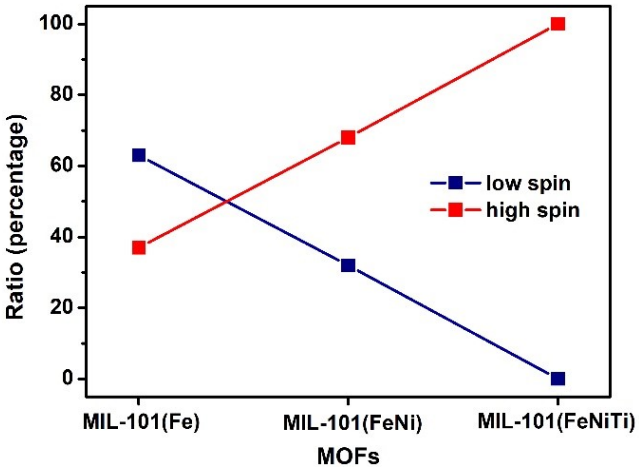

Figure S5. The transition tendency of spin states from MIL-101(Fe), MIL-101(FeNi) to MIL-101(FeNiTi).

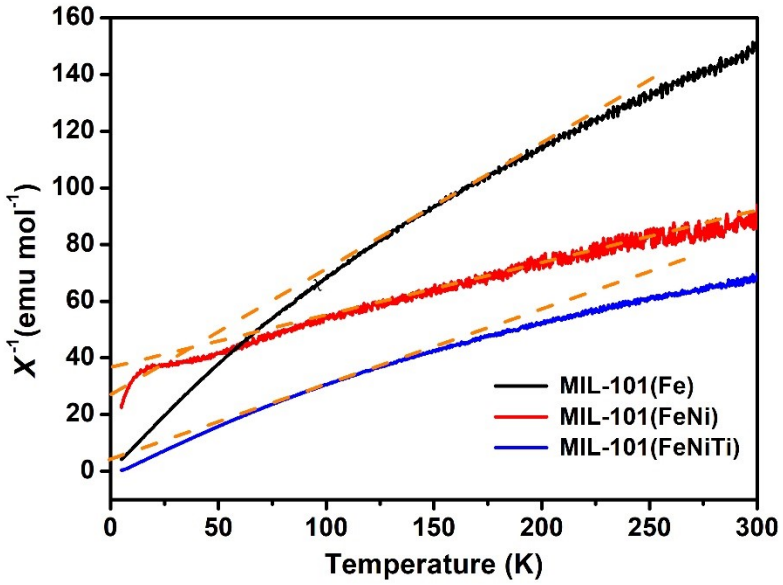

Figure S6. $1/\chi_m$ plots of MIL-101(Fe), MIL-101(FeNi) and MIL-101(FeNiTi).

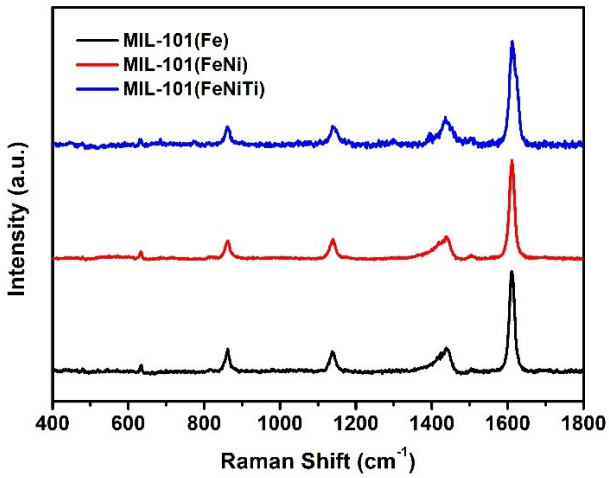

Figure S7. The Raman spectra of MIL-101(Fe), MIL-101(FeNi) and MIL-101(FeNiTi).

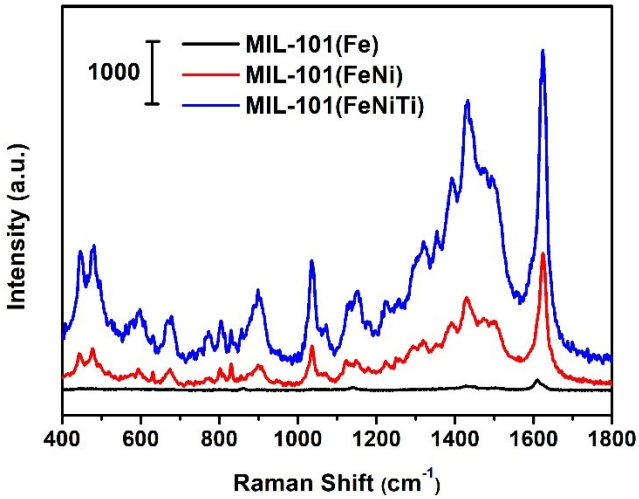

Figure S8. The SERS spectra of MB (10^{-5} M) adsorbed on three kinds of MOFs under 785 nm irradiation.

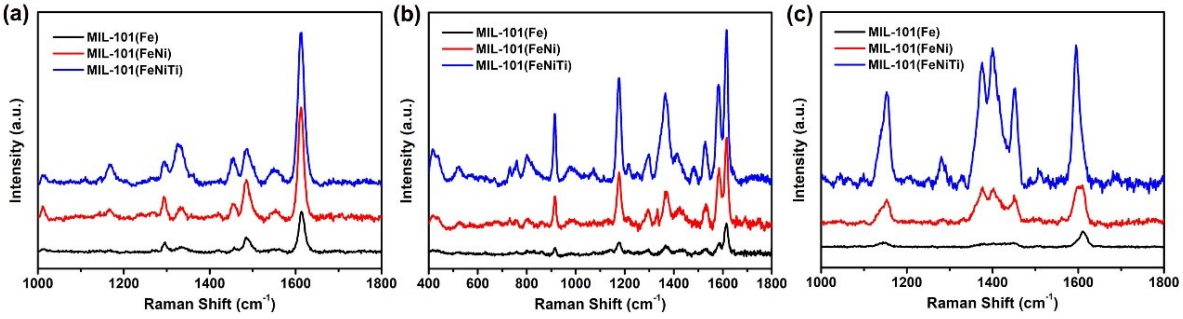

Figure S9. The SERS spectra of (a) Rose bengal (RB, 10^{-5} M) (b) Acid blue (AB, 10^{-5} M) and (c) Congo red (CR, 10^{-5} M) on trimetallic MIL-101(FeNiTi).

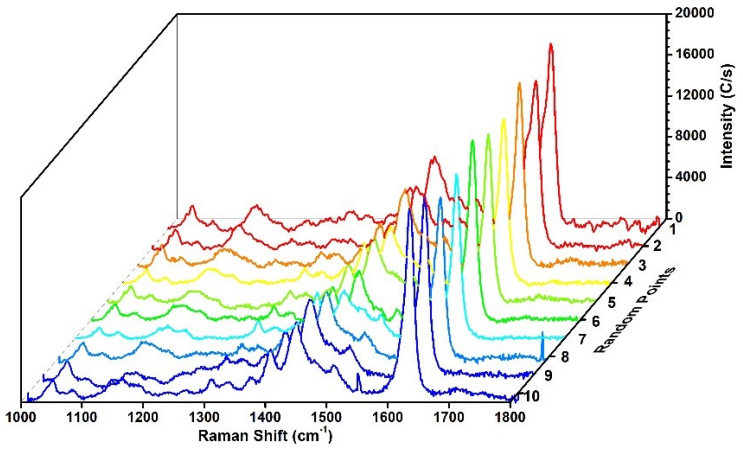

Figure S10. (a) The SERS spectra collected from 10 random positions on trimetallic MIL-101(FeNiTi).

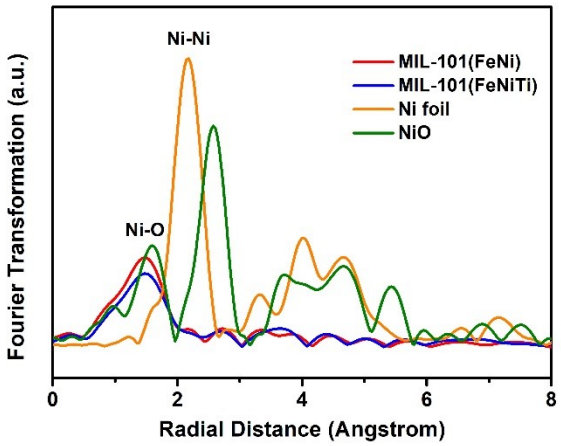

Figure S11. The k^3-weighted Fourier-transformed EXAFS spectra of Ni K-edge.

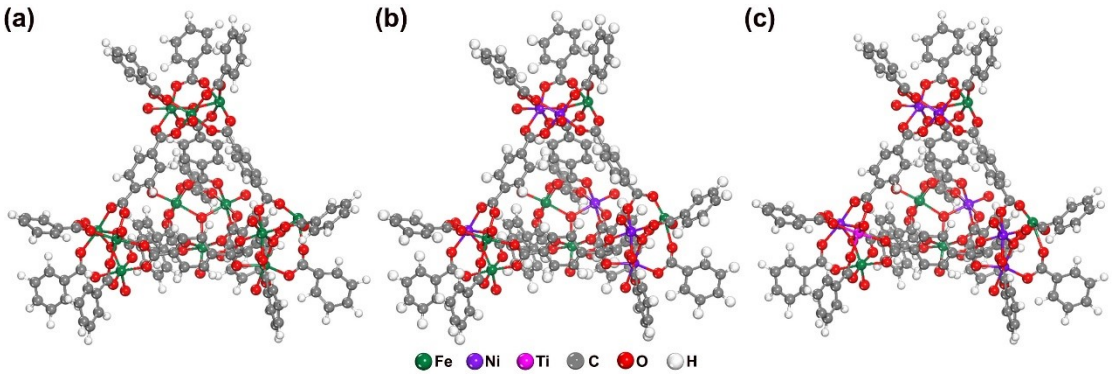

Figure S12. Schematic models of (a) MIL-101(Fe), (b) MIL-101(FeNi) and (c) MIL-101(FeNiTi).

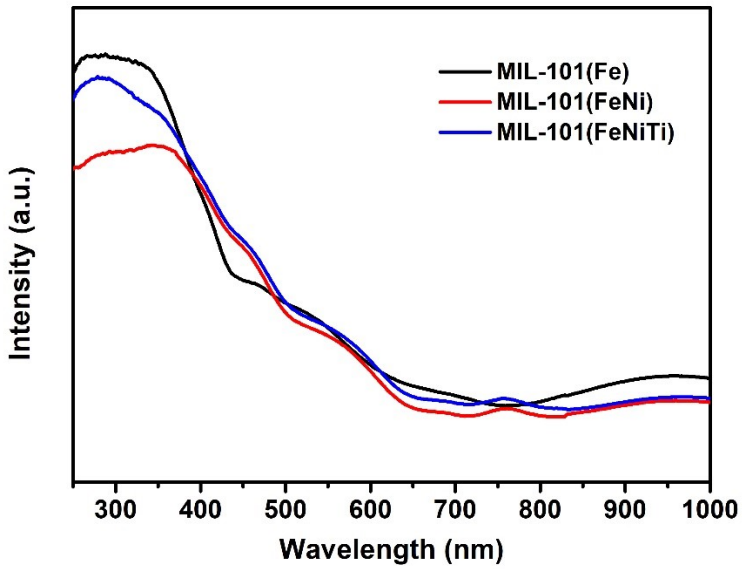

Figure S13. The UV-Vis absorption spectra of MIL-101(Fe), MIL-101(FeNi) and MIL-101(FeNiTi).

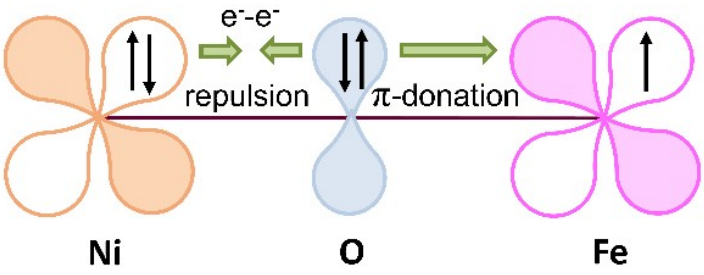

Figure S14. Schematic representation of the electronic coupling among Fe and Ni in MIL-101(FeNi).

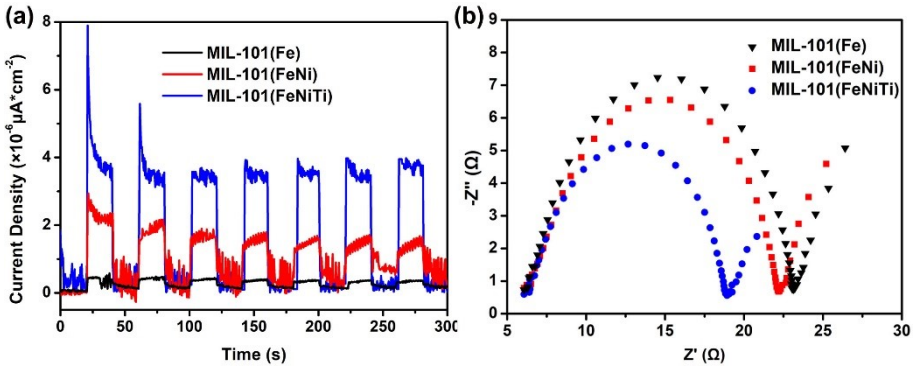

Figure S15. (a) Transient photocurrent test and (b) electrochemical impedance spectra of MIL-101(Fe), MIL-101(FeNi) and MIL-101(FeNiTi).

Calculation of the enhancement factor (EF)

The EF was calculated based on the following formula:

$$EF = (I_{SERS}/N_{SERS})/(I_{bulk}/N_{bulk}) \quad (1)$$

$$N_{SERS} = CVN_A A_{Raman}/A_{Sub} \quad (2)$$

$$N_{bulk} = N_A \rho h A_{Raman}/M \quad (3)$$

Where I_{SERS} and I_{bulk} are the intensities of the selected Raman peak (1625 cm^{-1}) in the SERS and non-SERS spectra, and N_{SERS} and N_{bulk} are the average number of molecules in the scattering area for SERS and non-SERS measurement. A_{sub} is the area of the substrate. The data for MB (10^{-2} M, aqueous solution) on bare glass was used as non-SERS-active reference. Specifically, the intensity was obtained by taking average from measurements of 30 spots, and the number of analyte molecules was estimated by Supplementary equation (2) on the assumption that the analyte molecules were distributed uniformly on the substrates. C is the molar concentration of the analyte solution, V is the volume of the droplet, N_A is Avogadro constant. A_{Raman} is the laser spot area (1 μm in diameter) of Raman scanning. Twenty microliters of the droplet on the substrate was spread into a circle of about 5 mm in diameter after solvent evaporation, from which the effective area of the substrate, A_{Sub}, can be obtained. The confocal depth (h) of the laser beam is 21 μm, and on the basis of molecular weight (M) and density (ρ) of bulk MB (1 g cm^{-3}), N_{bulk} is calculated by Supplementary equation (3), and the calculated EF according to equation (1) is 6.1×10^6.

Table S1 The inductively coupled plasma (ICP) measurement of the prepared MIL-101 (calculated as the moral ratios)

Substrates	ICP		
	Fe	Ni	Ti
MIL-101(Fe)	0.42	-	-
MIL-101(FeNi) (3:1)	0.31	0.11	-
MIL-101(FeNi) (2:1)	0.28	0.14	-
MIL-101(FeNi) (1:1)	0.21	0.20	-
MIL-101(FeNi) (1:2)	0.13	0.29	-
MIL-101(FeNi) (1:3)	0.11	0.31	-
MIL-101(FeTi) (1%)	0.40	-	0.02
MIL-101(FeTi) (2%)	0.38	-	0.04
MIL-101(FeTi) (4%)	0.34	-	0.08
MIL-101(FeTi) (6%)	0.31	-	0.11
MIL-101(FeTi) (8%)	0.28	-	0.14
MIL-101(FeNiTi) (1%)	0.20	0.19	0.02
MIL-101(FeNiTi) (2%)	0.19	0.19	0.03
MIL-101(FeNiTi) (4%)	0.17	0.17	0.08
MIL-101(FeNiTi) (6%)	0.15	0.15	0.12
MIL-101(FeNiTi) (8%)	0.14	0.13	0.15

Table S2 Hyperfine parameter and relative abundance of Fe-bearing phases.

Fe species	IS/mm s^{-1}	QS/mm s^{-1}	Area %	assignment
MIL-101(Fe)-D1	0.404	0.486	63.0	Fe^{III}, LS
MIL-101(Fe)-D2	0.414	0.901	37.0	Fe^{III}, HS
MIL-101(FeNi)-D1	0.399	0.602	32.1	Fe^{III}, LS
MIL-101(FeNi)-D2	0.415	0.968	67.9	Fe^{III}, HS
MIL-101(FeNiTi)-D2	0.433	0.867	100	Fe^{III}, HS

Table S3 Adsorption energy between MB and MIL-101(Fe), MIL-101(FeNi) and MIL-101(FeNiTi).

MB&	MIL-101(Fe)	MIL-101(FeNi)	MIL-101(FeNiTi)
Adsorption energy (eV)	-0.96	-1.46	-2.16

Reference

1 M. Zhao, K. Yuan, Y. Wang, G. Li, J. Guo, L. Gu, W. Hu, H. Zhao and Z. Tang, *Nature*, 2016, **539**, 76-80.

2 J. P. Perdew, K. Burke and M. Ernzerhof, *Phys. Review Lett.*, 1996, **77**, 3865-3876.

3 G. Kresse and J. Furthmüller, *Phys. Rev. B*, 1996, **54**, 11169.

4 G. Kresse and D. Joubert, *Phys. Rev. B*, 1999, **59**, 1758.

5 P. E. Blöchl, *Phys. Rev. B*, 1994, **50**, 17953.

6 S. Grimme, J. Antony, S. Ehrlich and H. Krieg, *J. Chem. Phys.*, 2010, **132**, 154104.

7 G. Henkelman, B. P. Uberuaga and H. Jónsson, *J. Chem. Phys.*, 2000, **113**, 9901-9904.

8 Y. Guo, C. Feng, S. Qiao, S. Wang, T. Chen, L. Zhang, Y. Zhao and J. Wang, *Nanoscale*, 2020, **12**, 12551-12560.

9 S. Qiu, Y. Wang, J. Wan, J. Han, Y. Ma and S. Wang, *Appl. Surf. Sci.*, 2020, **525**, 146511.

10 A. Khodkar, S. Khezri, A. Pendashteh, S. Khoramnejadian and L. Mamani, *Int. J. Environ. Sci. Technol.*, 2019, **16**, 5741-5756.

11 A. Jarrah and S. Farhadi, *J. Solid State Chem.*, 2020, **285**, 121264.

12 E. Amdeha and R. S. Mohamed, *Environ. Technol.*, 2021, **42**, 842-859.

13 N.N. Greenwood, T.C. Gibb. Mössbauer Spectroscopy Chapman and Hall, London (1971)